Journal of Materials Chemistry A

Accepted Manuscript

ROYAL SOCIETY OF CHEMISTRY

www.rsc.org/materialsA

Journal of Materials Chemistry A

Paper

Capsular polypyrrole hollow nanofibers: an efficient recyclable adsorbent for hexavalent chromium removal

Received 00th April 2015,
Accepted 00th January 2015

DOI: 10.1039/x0xx00000x

www.rsc.org/

Jian Zhao[a,c], Zhenyu Li[a], Jinfeng Wang[a,†], Quanxiang Li[a] and Xungai Wang[a,b, †]

Abstract Capsular polypyrrole hollow nanofibers (PPy-HNFs) were fabricated via in situ polymerization of pyrrole on an organic-inorganic template, followed by acid etching. Their application in removing hexavalent chromium (Cr (VI)) from aqueous solution was then investigated. Morphologies of the capsular PPy-HNFs were studied by both scanning electron microscopy (SEM) and transmission electron microscopy (TEM), which showed the PPy-HNFs had a capsular structure in the walls of hollow nanofibers. Fourier transform infrared (FTIR) spectroscopy and X-ray photoelectron spectroscopy (XPS) data confirmed the adsorption of Cr on capsular PPy-HNFs. The adsorption capacity increased with reduced pH of the initial solution and the adsorption process can be described using the pseudo-second-order model. This capsular PPy-HNFs showed a high Cr (VI) adsorption capacity up to 839.3 mg/g. This adsorption capacity was largely retained after five adsorption/desorption cycles. Electrostatic attraction between Cr and PPy-HNFs was studied with a proposed adsorption mechanism. The capsular PPy-HNFs formed a flexible membrane, which allowed easy handling during application. This study has demonstrated the possibilities of using this capsular PPy-HNFs membrane for heavy metal removal from aqueous solution.

1. Introduction

Water pollution by heavy metals is a growing concern. Since heavy metals have a high solubility in water and are widely used in different industries, it has become a global challenge to remove heavy metals from water in a highly efficient manner. As an example, Chromium (Cr) is widely used for electroplating, leather tanning, metal corrosion protection, and chrome pigments in textiles[1-3]. Cr is also listed as the second most abundant inorganic groundwater contaminant[4]. In aqueous solutions, Cr exists primarily in two valence states, trivalent (Cr (III)) and hexavalent (Cr (VI)). Cr (VI) is toxic for both acute and chronic exposures, whereas Cr (III) is a nutrient at trace levels[5]. Cr (VI) is considered to be a highly hazardous substance since it can cause critical health and environmental issues due to its carcinogenicity, mutagenicity, genotoxicity and bioaccumulation through the food chain. The World Health Organization (WHO) has recommended that the maximum allowable concentration for Cr (VI) in drinking water should be less than 0.05 ppm[6]. Therefore, it is necessary to reduce Cr (VI) concentration to an acceptable level in both potable water and industrial wastewater discharges for environment protection.

A wide range of technologies have been applied for Cr (VI) removal from aqueous solutions such as chemical precipitation[7], ion exchange[8] and membrane process[9]. However, each of the techniques has some drawbacks. Chemical precipitation generates a toxic sludge; there is a high cost associated with using ion-exchange resins; and the efficiency achieved by membrane treatments is often quite low. In contrast, adsorption is a versatile and cost-effective technique for Cr (VI) removal and has shown to be the most promising technique in recent years[10].

Many adsorbents, such as activated carbon[11], seaweed[12], cellulose[13], modified inorganic or organic porous materials[14-16], conducting polymers[17], have been extensively studied for Cr (VI) clean-up. Among these adsorbents, polypyrrole (PPy) has advantages of ease-synthesis, relatively low cost, and high adsorption capacity and efficiency[18]. PPy was first reported for Cr (VI) removal by Rajeshwar et al[19, 20]. Thereafter, many scientists focused on PPy derivatives and its composites for removing Cr (VI) from aqueous media. Rajeshwar et al[21] also fabricated PPy and carbon black alloy, which further increased Cr (VI) removal capacity. Gutiérrez and co-workers[22] deposited PPy on a graphite felt electrode. Lei et al reported PPy/cellulose fibers, which were fabricated by in situ

[a] Australian Future Fibres Research and Innovation Centre, Institute for Frontier Materials, Deakin University, VIC 3220, Australia
[b] School of Textile Science and Engineering, Wuhan Textile University, Wuhan 430073, China
[c] School of Textiles, State Key Laboratory of Separation Membranes and Membrane Processes, Tianjin Polytechnic University, Tianjin 300387, China
† These authors contributed equally to the work. Tel.: +61 3 52272894; Fax: +61 3 5227 1103. Email address: jinfeng.wang@deakin.edu.au (Jinfeng Wang); xungai.wang@deakin.edu.au (Xungai Wang).
Electronic Supplementary Information (ESI) available: details of any supplementary information available should be included here]. See DOI: 10.1039/x0xx00000x

polymerization[23]. More recently, nanosized PPy materials have attracted considerable attention because of their superior adsorptive properties. PPy nanoparticles[24, 25], PPy grafting silica gels[26], PPy/graphene oxide nanocomposites[27], polyacrylonitrile/PPy and PPy/polyaniline nanofibers[28, 29], and PPy-HNFs have been subsequently exploited. Among those PPy nanomaterials, hollow nanofibers became a new focal point because of its hollow characteristic and large storage capacity [30]. However, it is still a challenge to fabricate PPy-HNFs with controllable morphology and easy handling property during application.

In this study, PPy-HNFs were fabricated by polymerizing PPy on hollow vanadium pentoxide (V_2O_5) fibers and a subsequent acid etching technique was applied to remove the V_2O_5 template to obtain the capsular PPy-HNF membrane. The resulting material was used for removing Cr (VI) from aqueous solutions. The high surface area of the capsular PPy-HNFs promotes high adsorption capacity of Cr (VI). At the same time, the flexible membrane formed by PPy-HNFs provides easy handling for Cr (VI) removal from aqueous solutions. More importantly, the adsorbed Cr (VI) can be removed from capsular PPy-HNFs, allowing reuse of the capsular PPy-HNFs.

2. Experimental

2.1 Materials

Polyvinylpyrrolidone (PVP, M_w~1,300,000), N, N-dimethyl formamide (DMF), vanadyl acetylacetonate (VA, 98%), hydrogen chloride (37%), potassium dichromate (assay >99%) and pyrrole (Py, 98%) were purchased from Sigma-Aldrich. Polystyrene (PS, Mw~100,000) was from BDH chemical Ltd. Sodium hydroxide (analytical reagent) was provided by Chem-Supply Pty Ltd, Australia. All chemicals were used as received without further treatment.

2.2 Preparation of capsular PPy-HNFs

PS-(PVP/VA) core-shell nanofiber mat was prepared through electrospinning. In brief, VA and PVP were first dissolved in DMF, at 0.25 M and 0.15 g/mL, respectively. At the same time, PS was dissolved in DMF at a concentration of 0.2 g/mL. Subsequently, the above PVP/VA and PS solutions were mixed at a volume ratio of 3:2. The mixture was stirred for 12 h at a speed of 1500 rpm for electrospinning. The nanofibers were electrospun onto an aluminium foil at a DC voltage of 20 kV. The distance between the syringe needle (21 gauge) tip and the foil collector was 22 cm. The solution flow rate was 2 mL/h.

The prepared fiber mat was peeled off the collector and then sintered in air at 430 °C for 0.5 h to obtain the tubular V_2O_5. Then, vapour phase polymerization was conducted in desiccators. In a typical procedure, two beakers containing 2 mL of concentrated HCl or pyrrole monomer were placed into two separate desiccators labelled as A (HCl) and B (pyrrole). The resulting tubular V_2O_5 templates were first placed in the middle of the desiccator A. The desiccator was vacuum pumped for 10 min followed by gentle venting to acidify the V_2O_5 templates. The acidified V_2O_5 templates were then transferred to desiccator B and vacuumed for 1 h followed by gentle venting. This procedure was repeated for a second time, with dwelling time in desiccators A and B set for 1 h and 12 h, respectively. Finally, the residual V_2O_5 was removed (by immersing in HCl solution overnight) to obtain the capsular PPy-HNFs. Scheme 1 schematically shows the preparation process of the capsular PPy-HNFs.

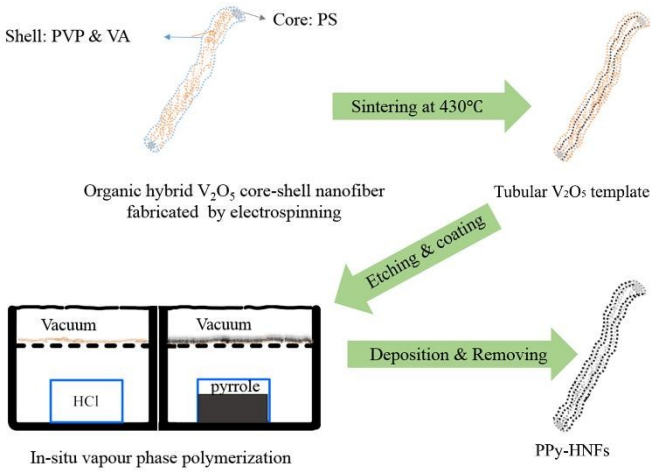

Scheme 1 Fabrication process of capsular PPy-HNFs.

2.3 Characterization

The morphologies and structure of tubular V_2O_5 templates and capsular PPy-HNFs were observed using a Supra 55VP (Zeiss, Germany) SEM operated at an acceleration voltage of 8.0 kV and a JEOL-2100 TEM with an acceleration voltage of 200 kV. Energy dispersive X-ray (EDX, Oxford Instruments, UK) spectra and EDX elemental mapping were also obtained. The specific surface area of capsular PPy-HNFs was determined using the IGC-Surface Energy Analyzer (Surface Measurement Systems, Alperton, Middlesex, UK) by octane adsorption isotherms at 30 °C and 0% RH. FTIR spectra were recorded on a Bruker VERTEX 70 instrument (Bruker Optics GmbH, Germany) using the KBr method. Thermal degradation data were collected by a thermogravimetric analyser (TGA) (Netzsch Inc., Germany) in air with a temperature ramp rate of 10 °C/min. Analysis of the X-ray photoelectron spectra (XPS) was performed on Thermo Electron Corporation ESCALAB 250 spectrometer with a Mg-K achromatic X-ray source (1253.6 eV). The zeta-potential of capsular PPy-HNFs at different pH was measured (Zeta-Sizer, Malvern Ltd., UK).

2.4 Adsorption studies of Cr (VI)

Cr (VI) solutions were prepared by dissolving $K_2Cr_2O_7$ in deionized water. The concentration of the Cr (VI) stock solution was adjusted to 1000 ppm. Adsorption procedures were conducted at different concentrations by diluting the stock solution.

The pH value of the solutions (from 2 to 10) was adjusted using a TPS WP-81 pH meter (TPS Ionode, Australia) by adding hydrochloric acid (HCl) and sodium hydroxide (NaOH). 30 mg of capsular PPy-HNFs were added into 200 mL of 200 ppm Cr (VI) solutions. The

above mixture was then placed in a thermo-static shaker (Ratek SWB20D, AU) agitated at 300 rpm and at ambient temperature (25±1℃) for 24 h. The concentration of the residual Cr (VI) in the solution was characterized by Cary 5000 UV−vis spectrophotometer (Varian Co., US) with the wavelength at 370 nm. Removal efficiency of Cr (VI) was determined using Equation (1):

$$\textbf{Removal efficiency}\ (\%) = \frac{C_0 - C_e}{C_0} \times 100 \quad (1)$$

where C_0 is the initial concentration, C_e is the equilibrium concentration.

To investigate the kinetic characteristics of the adsorption process, 30 mg of capsular PPy-HNFs were added into 200 mL of Cr (VI) solution with different concentrations (75, 150 and 200 ppm) at pH=2. The residual concentrations of Cr (VI) were measured after certain time intervals. The adsorption capacity q_t (mg/g) was calculated according to Equation (2):

$$\textbf{Adsorption capacity}\ (q_t)\ (mg/g)) = \frac{C_0 - C_t}{m} \times V \quad (2)$$

where, C_0 is the initial concentration; C_t is the residual concentration of Cr (VI) at time *t*; *V* is the volume of Cr (VI) solution; *m* is the weight of capsular PPy-HNFs. q_t is the adsorption capacity at time *t*. After the adsorption for 24 h, equilibrium adsorption capacity (q_e) was achieved. The change of pH in the Cr (VI) solution was monitored during the adsorption process. The Cr concentration in the residual solution was measured with a Varian 715-ES inductively coupled plasma-atomic emission spectrometer (ICP-AES, Varian 715-ES, Agilent Technologies, CA, USA) (See ICP-ES results in supporting information).

The effect of initial concentration (50, 100, 200, 300, 400, 500, 600 ppm) of Cr (VI) on adsorption capacity of PPy-HNFs was also investigated. The experiment was performed at pH=2, by immersing 30 mg capsular PPy-HNFs into 200 mL Cr (VI) solution, and agitating in a thermo-static shaker at 300 rpm for 8 h.

The adsorption–desorption cycles were repeated consecutively for 5 times to determine the reusability of capsular PPy-HNFs. The adsorption experiments were carried out under the following conditions: volume, 200 mL; adsorbent dosage, 30 mg; initial concentration, 200 ppm; pH= 2; adsorption time, 8 h; temperature, 25 °C; agitation speed, 300 rpm. In each cycle, the capsular PPy-HNFs were separated from the solution after adsorption of Cr (VI) and then soaked in 50 mL NaOH aqueous solutions for 3 h. Three different NaOH solutions were applied for the Cr (VI) desorption process, at concentrations of 0.1 M, 0.5 M, and 1M, respectively. Adsorbents were rinsed with 0.1 M HCl and deionized water before the second adsorption cycle. The adsorption capacity of capsular PPy-HNFs for each cycle was determined by Equation 2.

3. Results and discussion

3.1. Morphology of capsular PPy-HNFs

Figures 1a and 1b show the morphology of the tubular V_2O_5 templates. The tubular templates of V_2O_5 were obtained based on PS-(PVP/VA) core-shell nanofiber (See Figure S1 & explanation of core-shell structure in supporting information). The walls of V_2O_5 templates were stacked by V_2O_5 nanoparticles, like squid carved roll. Most of V_2O_5 nanoparticles are less than 100 nm with an irregular prismatic shape. The initial yellow V_2O_5 templates turned black after the polymerization (See Figure S2 in supporting information), which indicated the formation of PPy on the surface of V_2O_5 nanoparticles. The V_2O_5 nanoparticles were removed by HCl etching to obtain the hollow nanofibers with PPy nanocapsules in the wall. As shown in Figure 1c, each capsule is around 100 nm, with the capsular wall thickness of about 20 nm. The capsular PPy-HNFs formed a flexible 3D PPy-HNF membrane, which could provide easy handling for Cr (VI) adsorption applications (see Video S1 in supporting information). The hollow templates (Figure 1a &b), as a growing substrate, caused many capsular bulges in the walls of PPy-HNFs as shown in Figure 1d, which resulted in a large surface area. Brunauer-Emmett-Teller (BET) surface area of capsular PPy-HNFs was found to be 47.9 m^2/g from surface energy results (See Figure S3 in supporting information), which is almost twice as large as PPy powder of 23 m^2/g [31] and PPy film of 25.2 m^2/g [32]. It is also larger than the conventional PPy nanoparticles of 41.3 m^2/g [33]. The capsular and tubular morphology of PPy-HNFs provides a capillary effect, which acts as a driving force for the Cr (VI) adsorption. Meanwhile, the increased surface area of capsular PPy-HNFs prompts a large storage area for heavy metal adsorption.

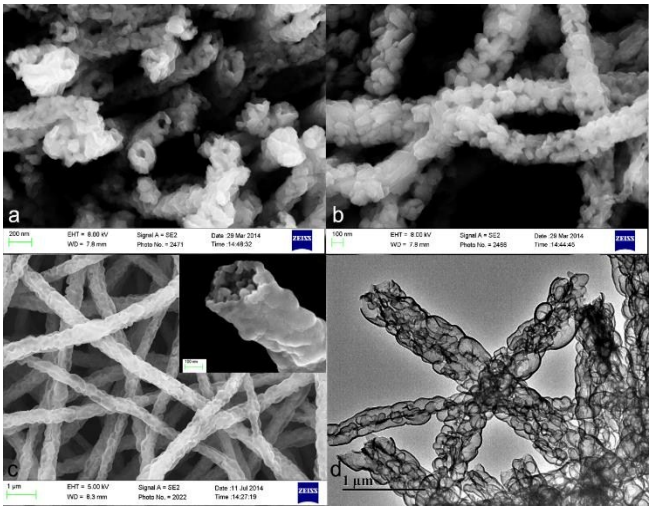

Fig. 1 SEM images of cross section (a) and surface morphology (b) of tubular V_2O_5 templates, (c) capsular PPy-HNFs, inset is the cross section of the capsular PPy-HNFs, (d) TEM image of the typical capsular PPy-HNFs.

3.2. Adsorption of Cr (VI) by capsular PPy-HNFs

The presence of Cr (VI) on capsular PPy-HNFs after adsorption was verified by SEM-EDX technique as shown in Figure 2. Two strong peaks were observed at 0.6 keV and 5.4 keV in EDX spectra, which were identified as Cr (VI). The amount of Cr (VI) on capsular PPy-HNFs was also measured by X-ray elemental mapping. The quantitative analysis depicts the compositions calculated from the peak areas, and the results are labelled in the inset of Figure 2. Specifically, O and N come from PPy-HNFs, and Cl is mainly from HCl during acid etching process. It can be clearly observed that PPy-HNFs contain a high amount of Cr (VI) after adsorption. The total content of Cr (VI) on PPy-HNFs was found to be 41.75 wt. % after adsorption.

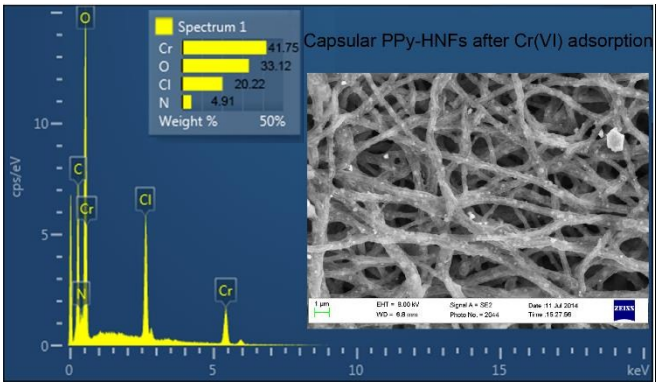

Fig. 2 EDX spectra & SEM image (shown on right set) of capsular PPy-HNFs after adsorption (the adsorption was carried out at Cr (VI) concentration of 200 ppm and pH=2).

The adsorption of Cr (VI) on capsular PPy-HNFs was further confirmed by FTIR. Figure 3 shows the FTIR spectra of the capsular PPy-HNFs before and after Cr (VI) adsorption. The peaks of 3408 and 3128 cm^{-1} reveal the presence of the N-H band. The characteristic absorption bands of capsular PPy-HNFs are assigned as follows: 1545 cm^{-1} for C=C stretching of pyrrole ring, 1452 and 1400 cm^{-1} for C=N stretching and in-plane deformation, 1298 and 1043 cm^{-1} for =C-H in-plane vibrations and C-H outer-bending vibrations, 1173 cm^{-1} for pyrrole ring breathing, 900 cm^{-1} for ring deformation associated with bipolarons and polarons, respectively [34]. These peaks are consistent with the reported results[25, 35]. While the other peaks, the frequencies centred at 1630~1708 cm^{-1} are considered to arise from C=O, which may result from PPy peroxidation[36]. The FTIR spectrum of the capsular PPy-HNFs after Cr (VI) adsorption (Cr@PPy-HNFs) demonstrated peaks at 3381, 3226, 1573, 1213, 1051 and 932 cm^{-1}, which are the signatures of pyrrole ring [24]. Some spectroscopic differences are observed in the 1500–1300 cm^{-1} region after Cr (VI) adsorption, which are the signature of $K_2Cr_2O_7$ infrared absorption bands [37]. Compared to the spectra of capsular PPy-HNFs before adsorption, most of the peaks shifted to higher wavenumbers after Cr (VI) adsorption. This change may be attributed to the existence of various types of Cr (VI) on PPy-HNFs, which agitate the conjugate structure of the PPy and limit the extent of polymer chain charge delocalization, hence resulting in peaks shifting to higher adsorption wavenumbers [24].

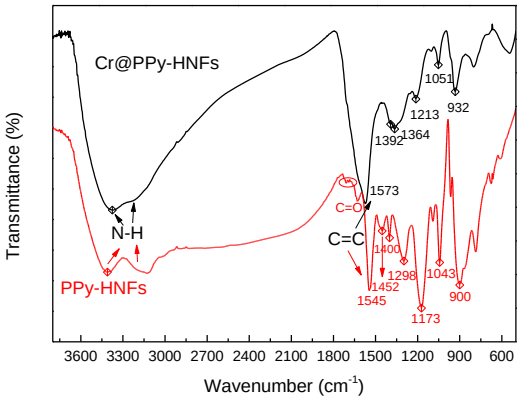

Fig. 3 FTIR spectra of capsular PPy-HNFs before and after Cr (VI) adsorption.

The loading levels of the Cr (VI) on capsular PPy-HNFs were determined by TGA. Figure 4 shows the mass loss of capsular PPy-HNFs before and after Cr (VI) adsorption. The weight loss of capsular PPy-HNFs below 150 °C corresponded to water loss. A major mass loss region for capsular PPy-HNFs was found from 230°C to 620 °C, which was attributed to polymer degradation. Compared to PPy-HNFs before Cr (VI) adsorption, a greatly weight loss was observed before 360 ◦C for PPy-HNFs after adsorption of Cr (VI). This lower degradation temperature may be caused by the incorporation of metal ions Cr into the PPy structure, which leads to a reduced thermal stability. A similar result was report by Baroni et al [38]. Compared to 2.9 wt. % residual left for the capsular PPy-HNFs after 620°C, 25.6 wt. % residue weight was found for Cr (VI) adsorbed capsular PPy-HNFs. This result further confirms the presence of Cr (VI) in capsular PPy-HNFs after adsorption.

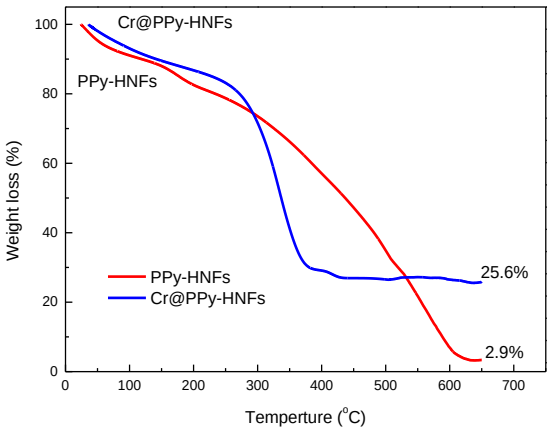

Fig. 4 TGA curves of capsular PPy-HNFs before and after Cr (VI) adsorption.

3.3. pH effect on adsorption capacity of capsular PPy-HNFs

The pH effect on the adsorption capacity of capsular PPy-HNFs was investigated by varying pH from 2 to 10. It was found that the adsorption capacity of capsular PPy-HNFs increased with decreasing

pH. As shown in Figure 5, the Cr (VI) removal efficiency was higher than 90% at pH =2, which decreased sharply when pH is higher than 6. Almost no removal efficiency was found at pH 10. According to literature, Cr (VI) predominantly exists as $HCrO_4^-$ and $Cr_2O_7^{2-}$ in aqueous solution when the pH is in the range of 2-6. When the pH is above 6, the dominant species is CrO_4^{2-} [11]. From the electrostatic interaction point of view, PPy has predominately Lewis acidity, with the acidic sites possibly being the most energetic. The charged $-NH^+$ groups are enhanced at low pH and become more positively charged, while high pH leads to the negative surface charge due to deprotonation[39]. Therefore, the reason for the decrease of adsorption efficiency with increased pH is due to the competitive interaction between CrO_4^{2-} and OH^- ions for the same adsorption sites on the adsorbent surface. On the other hand, partial Cr (VI) was reduced by the electron rich polymer matrix to Cr (III) as represented in XPS results (see Section 3.7), and further possibly formed chromium hydroxide ($Cr(OH)_3$). Compared with Cr (VI), $Cr(OH)_3$ flocculation was difficult to be adsorbed. Finally, the capsular PPy-HNFs showed the highest Cr (VI) removal efficiency of 90.8% when pH was 2. Therefore, the subsequent adsorption experiments were all carried out at pH 2.

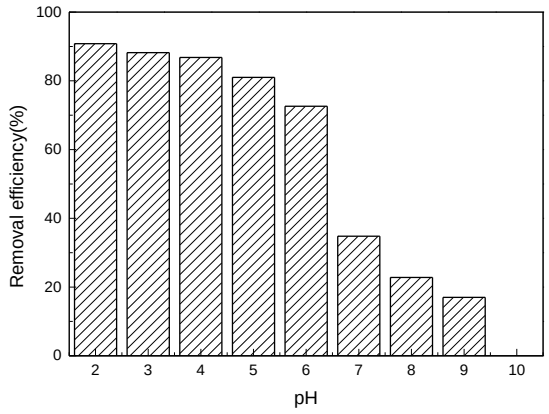

Fig. 5 Cr (VI) removal efficiency under different pH (from 2 to 10).

3.4. Effects of initial concentrations of Cr (VI) on adsorption capacity of capsular PPy-HNFs

The adsorption capacity of capsular PPy-HNFs with different initial concentrations of Cr (VI) can be used to reflect actual usage of the adsorbent. The adsorption capacity of the capsular PPy-HNFs increased with the increasing initial concentration of Cr (VI). As shown in Figure 6, the adsorption capacity was 333 mg/g when Cr (VI) concentration was 50 ppm. The adsorption capacity increased to 1386 mg/g at Cr (VI) concentration of 600 ppm. However, reduced removal efficiency was verified with increasing Cr (VI) concentration. The dosage of 150 mg/L PPy-HNFs can achieve almost 100% Cr (VI) removal efficiency with concentration of Cr (VI) less than 100 mg/L. Further increase of the initial concentration of Cr (VI) resulted in reduced removal efficiency.

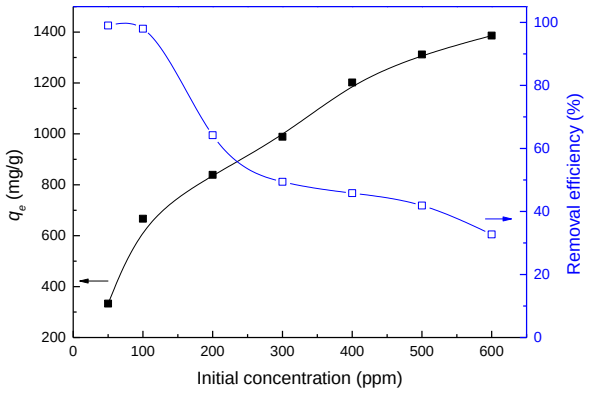

Fig. 6 Effects of different initial concentrations of Cr (VI) on adsorption capacity of capsular PPy-HNFs and Cr (VI) removal efficiency.

3.5. Adsorption kinetics

The effects of adsorption time on the adsorption capacity of capsular PPy-HNFs at different initial concentrations of Cr (VI) are shown in Figure 7. The adsorption capacity increased rapidly in the first 30 mins and then gradually reaches plateau, indicating the Cr (VI) adsorption was nearly complete in 8 h. The rapid uptake in the first 30 mins indicates a high affinity between Cr (VI) and the capsular PPy-HNFs, which was attributed to the large specific surface area of capsular PPy-HNFs and the capillary effect promoting the rapid mass diffusion and transport. The color of 150 mg/L Cr (VI) solution changed from golden yellow to nearly colorless after 24 h adsorption.

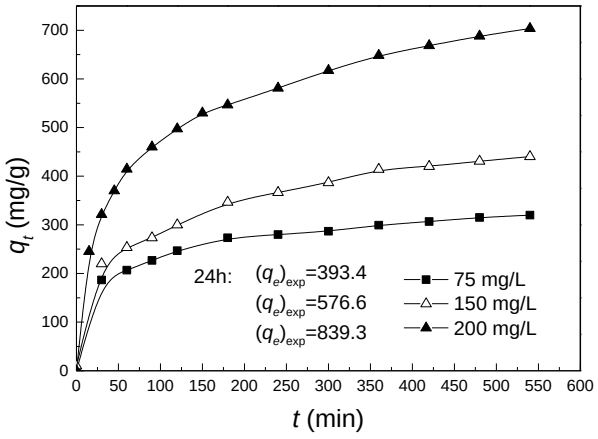

Fig. 7 Effects of adsorption time on Cr (VI) adsorption capacity with different initial concentrations.

To better understand the adsorption process, adsorption kinetics was investigated according to two commonly used models, the pseudo-first-order model and the pseudo-second-order model. These two kinetic models have been used to describe the adsorption of liquid/solid systems, which are expressed in Equations (3) [40, 41] and (4) [42, 43], respectively:

$$log(q_e - q_t) = log q_e - \frac{k_1}{2.303} t \quad (3)$$

$$t/q_t = 1/k_2 q_e^2 + t/q_e \quad (4)$$

where q_t and q_e refer to the value of adsorption capacity (mg/g) at certain time t (min) and after equilibrium, respectively; k_1 and k_2 are the pseudo-first-order and pseudo-second-order rate constants.

The slope and intercept of the plots of log (q_e−q_t) versus t are used to determine the rate constant for pseudo-first-order, while the slope and intercept of the plots of t/q_t versus t are used for the pseudo-second-order rate constant (see Supporting Information Figure S4 and S5). The obtained kinetic parameters are summarized in Table 1. The values of correlation coefficients clearly demonstrate that the adsorption kinetics follow the pseudo-second-order model, with correlation coefficients higher than 0.98. The pseudo-second-order rate constant (k_2) decreased from 7.23×10^{-5} to 2.52×10^{-5} when the initial Cr (VI) concentration increased from 75 mg/L to 200 mg/L.

Table 1 Kinetic parameters for Cr (VI) adsorption by capsular PPy-HNFs.

Initial Cr (VI) concentration	$(q_e)_{exp}$	Pseudo-first-order			Pseudo-second-order		
		$(q_e)_{cal}$	k_1	R^2	$(q_e)_{cal}$	k_2	R^2
75	393.4	229.8	2.40×10^{-3}	0.816	337.8	7.23×10^{-5}	0.997
150	576.6	391.1	2.21×10^{-3}	0.885	463.0	4.73×10^{-5}	0.995
200	839.3	550.7	2.86×10^{-3}	0.917	751.9	2.52×10^{-5}	0.988

Table 2 summarized the adsorption performance of Cr (VI) by different PPy adsorbents reported by literatures. The capsular PPy-HNFs have an exceptional adsorption capacity of 839.3 mg/g, which is superior to all the other PPy adsorbents reported. To the best of our knowledge, this is the highest adsorption capacity among all the reported adsorbents under the given conditions (pH=2).

Table 2 Comparison of adsorption performance of PPy adsorbents for Cr (VI) in the last decade.

Adsorbents	Type and method	Max adsorption capacity	Ref.
PPy/Cellulose composite	Fibers, coated polymerization	~130 mg/g for 200 ppm	23
PPy-organically modified montmorillonite clay nanocomposite	Nanosheets, in situ polymerization	69.1mg/g for 200 ppm	24
PPy/Fe_3O_4 nanocomposite	Nanoparticles, chemical polymerization	230.2mg/g for 100 ppm	25
PPy grafting with silica gel	Nanoparticles, ether catalyse graft	~18 mg/g for 45 ppm	26
PPy/graphene oxide composite	Nanosheets, sacrificial-template deposition	497.1 mg/g for 579.5 ppm	33
PAN/PPy core/shell mats	Nanofibers, in situ polymerization	61.8 mg/g for 200 ppm	28
PPy-PANI nanofibers	Nanofibers, chemical oxidative synthesis	227-294 mg/g for 100-400 ppm	29
(PPy-O)Cl_2	Bulk powder, precipitated polymerization	~17 mg/g for 85 ppm	44
Fe_3O_4@glycine doped PPy magnetic nanocomposites	Nanoparticles, in situ polymerization	238 mg/g for 200 ppm	45
Capsular PPy-HNFs	Hollow nanofibers, vapour phase polymerization based on inorganic assisted template	839.3 mg/g for 200 ppm	This study

Journal of Materials Chemistry A

Paper

3.6. Reusability of capsular PPy-HNFs

The reusability of the PPy-HNFs was investigated by performing several cycles of Cr (VI) adsorption and desorption. The Cr (VI) desorption from capsular PPy-HNFs was achieved by NaOH washing at different concentrations. Capsular PPy-HNFs regenerated by 0.1 M NaOH deteriorated in adsorption, especially after 3 cycles. This is possibly because the low concentration of alkaline is insufficient to completely desorb Cr (VI) from capsular PPy-HNFs. 0.5 M NaOH enhanced regeneration of the adsorption capacity of PPy-HNFs. 839.3mg/g of Cr (VI) adsorption capacity was reached in the first cycle and 75% of the adsorption capacity was maintained after five adsorption and desorption cycles. Further increase of NaOH concentration to 1.0 M resulted in a significant decrease in the adsorption capacity of capsular PPy-HNFs even after the first time use, which could be attributed to the instability of capsular PPy-HNFs under a high alkaline condition. It was found that the capsular structure of the PPy-HNFs partially collapsed and part of the PPy-HNFs dissolved after soaking in a high alkaline solution (see Supporting Information Figure S6 & Figure S7). Therefore, 0.5 M NaOH was found to be the optimum condition for regenerating the capsular PPy-HNFs for Cr (VI) removal from aqueous solution.

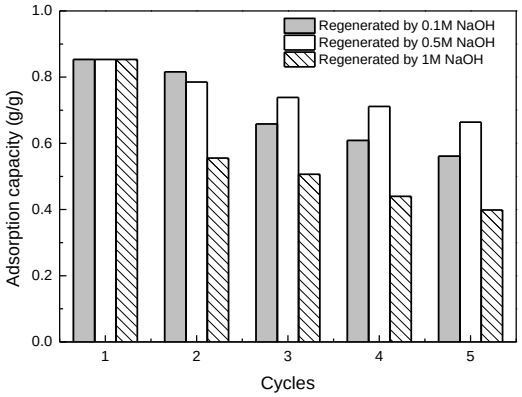

Fig. 8 Adsorption-desorption cycles at different alkali concentrations.

3.7. Adsorption mechanism

The adsorption mechanism of Cr (VI) on PPy-HNFs was studied by XPS. Compared to the capsular PPy-HNFs before adsorption, two new energy bands were observed after Cr adsorption, which were at 577.5 eV and 587.2 eV, respectively. These two energy bands corresponded to the binding energies of Cr ($2p_{3/2}$) and Cr ($2p_{1/2}$) [25]. The presence of Cr ($2p_{3/2}$) and Cr ($2p_{1/2}$) confirms the existence of both Cr (III) and Cr (VI) on the surface of capsular PPy-HNFs. The presence of Cr (III) on the surface of capsular PPy-HNFs suggests that some adsorbed Cr (VI) was reduced to Cr (III). The reduction may be attributed to the presence of positive $-NH^+$ group in PPy-HNFs [28]. The fraction of Cr (VI) and Cr (III) in adsorbents was calculated using peak fitting method by subtracting baseline and integration. The integral area ratio of the peaks of Cr (VI) and Cr (III) was calculated to be 2:3, which indicates that 60% of the total adsorbed Cr (VI) was reduced to be Cr (III) on the surface of PPy-HNFs. The reduction of Cr (VI) to be Cr (III) after adsorption are in agreement with result presented in other literatures [46, 47].

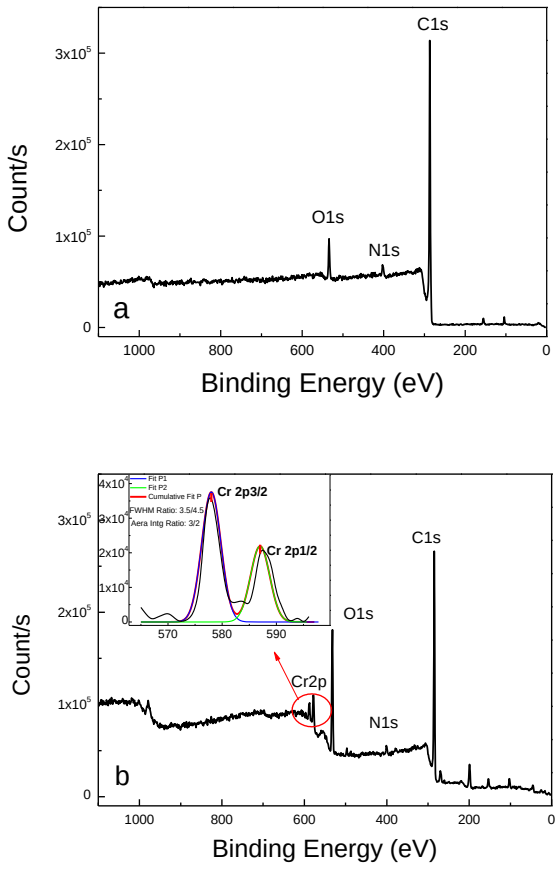

Fig. 9 XPS spectra of capsular PPy-HNFs before (a) and after (b) Cr adsorption.

The isoelectric point (pI) and pH changes of capsular PPy-HNFs were also used to investigate Cr (VI) adsorption mechanism. As mentioned above, Cr (VI) predominantly exists as $HCrO_4^-$ and $Cr_2O_7^{2-}$ when pH is less than 6; while the dominant species is CrO_4^{2-} when the pH is above 6. As shown in Table 3, the pI of capsular PPy-HNFs was estimated to be in the pH range of 5-6.The PPy-HNFs is

positively charged at pH < pI, which promotes its electrostatic attraction with negatively charged $HCrO_4^-$ /$Cr_2O_7^{2-}$. While at pH > pI, PPy-HNFs became negatively charged, which prevents its interaction with CrO_4^{2-}, resulting in reduced adsorption capacity. We suggest that this electrostatic attraction between protonated amine groups and $HCrO^{4-}$ groups provides the ablility of Cr (VI) removal from water.

Table 3 Zeta potential of PPy-HNFs at different pH values.

pH	3	4	5	6	7	8	9
Zeta potential (mV)	8.02	3.5	1.18	-3.05	-11.5	-13.4	-16.6

pH of the solution increased rapidly from 2.00 to 2.02 in the first 2 h and then gradually reached its equilibration at pH of 2.04. This result indicates a large amount of H^+ ions were consumed during the Cr adsorption process (Figure 10). The consumption of H^+ can be attributed to the protonation of amine groups of PPy-HNFs and the reduction of Cr (VI) into Cr (III) according to equations (5) and (6) [48, 49]:

$$HCrO_4^- + 7H^+ + 3e \leftrightarrow Cr^{3+} + 4H_2O \quad (5)$$

$$Cr_2O_4^- + 14H^+ + 6e \leftrightarrow 2Cr^{3+} + 7H_2O \quad (6)$$

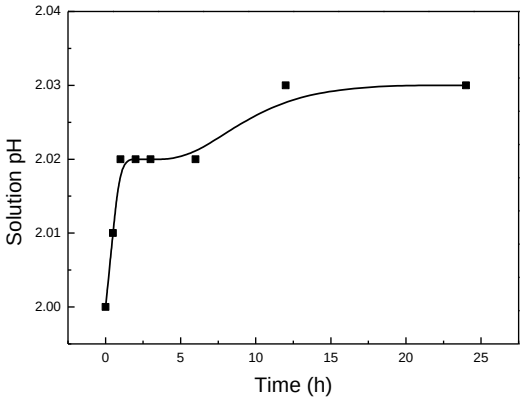

Fig. 10 Variation of solution pH during the Cr (VI) removal by PPy-HNFs. (Adsorbent feed: 200 ppm Cr (VI) solution, pH=2).

4. Conclusions

In this study, reusable polypyrrole hollow nanofibers (PPy-HNFs) with a capsular wall were fabricated using an inorganic template and vapour phase polymerization approach. The capsular PPy-HNFs showed a significantly high adsorption capacity for heavy metal Cr (VI), up to 839.3 mg/g for 200 ppm at pH=2. Adsorption kinetics suggested the adsorption follows the pseudo-second-order model. Sodium hydroxide solution can be used to recover the adsorption capacity of the capsular PPy-HNFs. The capsular PPy-HNFs maintained the impressive adsorption capacity after five cycles of adsorption/desorption process. Electrostatic attraction between PPy-HNFs and chromium was confirmed during Cr (VI) removal. The capsular PPy-HNFs formed a flexible membrane, which allowed easy handling during application. This capsular PPy-HNFs membrane may have great potential for removal of heavy metals from industrial effluents and other water sources.

Acknowledgements

The authors thank Jock Christoe for editing English of this paper.

References

1 E.V. Skorb and D.V. Andreeva, Adv. Funct. Mater., 2013, **23**, 4483-4506.
2 F. Cao, K. McEnaney, G. Chen and Z. Ren, Energ. Environ. Sci., 2014, **7**, 1615-1627.
3 B. Qiu, H. Gu, X. Yan, J. Guo, Y. Wang, D. Sun, Q. Wang, M. Khan, X. Zhang, B. L. Weeks, D. P. Young, Z. Guo and S. Wei, J. Mater. Chem. A., 2014, **2**, 17454-17462.
4 D. Blowes, Science., 2002, **295**, 2024-2025.
5 A. Zhitkovich, Chem. Res. Toxicol., 2011, **24**, 1617-1629.
6 W.H.O., Guidelines for drinking-water quality, fourth ed., WHO Press, Geneva, 2011.
7 N. Meunier, P. Drogui, C. Montané, R. Hausler, G. Mercier and J.-F. Blais, J. Hazard. Mater., 2006, **137**, 581-590.
8 J. Hu, P. Tao, S. Wang, Y. Liu, Y. Tang, H. Zhong and Z. Lu, J. Mater. Chem. A., 2013, **1**, 6558-6552.
9 L. Guo, Y. Liu, C. Zhang and J. Chen, J. Membra. Sci., 2011, **372**, 314-321.
10 L. Zhang, W. Xia, X. Liu and W. Zhang, J. Mater. Chem. A., 2015, **3**, 331-340.
11 T. Karthikeyan, S. Rajgopal and L.R. Miranda, J. Hazard. Mater., 2005, **124**, 192-199.
12 D. Kratochvil, P. Pimentel and B. Volesky, Environ. Sci. Technol., 1998, **32**, 2693-2698.
13 Y. Zhou, Q. Jin, T. Zhu and Y. Akama, J. Hazard. Mater., 2011, **187**, 303-310.

14 J. Zhu, H. Gu, J. Guo, M. Chen, H. Wei, Z. Luo, H. A. Colorado, N. Yerra, D. Ding, T. C. Ho, N. Haldolaarachchige, J. Hopper, D. P. Young, Z. Guo and S. Wei, J. Mater. Chem. A., 2014, **7**, 2256-2265.
15 K. Bhowmik, A. Mukherjee, M.K. Mishra and G. De, Langmuir., 2014, **30**, 3209-3216.
16 Z. Huang, B. Zhang and G. Fang, BioResources. 2013, **8**, 4593-4608.
17 K.K. Krishnani, S. Srinives, B.C. Mohapatra, V.M. Boddu, J.M. Hao, X. Meng and A. Mulchandani, J. Hazard. Mater., 2013, **252**, 99-106.
18 C. Li, C. Sun, W. Chen and L. Pan, Surf. Coat. Technol., 2005, **198**, 474-477.
19 C. Wei, S. German, S. Basak and K. Rajeshwar, J. Electrochem. Soc., 1993, **140**, L60-L62.
20 R. Senthurchelvan, Y. Wang, S. Basak and K. Rajeshwar, J. Electrochem. Soc., 1996, **143**, 44-51.
21 W.A. Wampler, S. Basak, K. Rajeshwar, Carbon., 1996, **34**, 747-755.
22 M.A. Alatorre, S. Gutierrez, U. Paramo and J.G. Ibanez, J. Appl. Electrochem., 1998, **28**, 551-557.
23 Y. Lei, X.R. Qian, J. Shen and X.H. An, Ind. Eng. Chem.Res., 2012, **51**, 10408-10415.
24 K.Z. Setshedi, M. Bhaumik, S. Songwane, M.S. Onyango and A. Maity, Chem. Eng. J., 2013, **222**, 186-197.
25 M. Bhaumik, A. Maity, V.V. Srinivasu and M.S. Onyango, J. Hazard. Mater., 2011, **190**, 381-390.
26 P. Mondal, K. Roy, S.P. Bayen and P. Chowdhury, Talanta., 2011, **83**, 1482-1486.
27 Setshedi, K. Z., M. Bhaumik, M. S. Onyango and A. Maity, Chem. Eng. J., 2015, **262**, 921-931.
28 J.Q. Wang, K. Pan, Q.W. He and B. Cao, J. Hazard. Mater., 2013, **244**, 121-129.
29 M. Bhaumik, A. Maity, V.V. Srinivasu and M.S. Onyango, Chem. Eng. J., 2012, **181**, 323-333.
30 S. Li, X. Lu, X. Li, Y. Xue, C. Zhang, J. Lei and C. Wang, J. Colloid. Interf. Sci., 2012, **378**, 30-35.
31 K.H. An, S.Y. Jeong, H.R. Hwang and Y.H. Lee, Adv. Mater., 2004, **16**, 1005-1009.
32 T.H. Chao and J. March, J. Polym. Sci. A., 1988, **26**, 743-753.
33 S.K. Li, X.F. Lu, Y.P. Xue, J.Y. Lei, T. Zheng and C. Wang, Plos One., 2012, **7**, e43328.
34 H.S. Kim, D.H. Park, Y.B. Lee, D.-C. Kim, H.-J. Kim, J. Kim and J. Joo, Synthetic Met., 2007, **157**, 910-913.
35 L. Cui, J. Li and X.G. Zhang, Mater. Lett., 2009, **63**, 683-686.
36 G.I. Mathys and V.T. Truong, Synthetic Met., 1997, **89**, 103-109.
37 R.A. Nyquist and R.O. Kagel, Infrared spectra of inorganic compounds, in: UK (Ed.), Handbook of infrared and raman spectra of inorganic compounds and organic salts, Academic Press Inc., London, 1971, 1-18.
38 2 P. Baroni, R. S. Vieira, E. Meneghetti, M. G. C. da Silva and M. M. Beppu, J. Hazard. Mater., 2008, **152**, 1155-1163.
39 M.J. Higgins and G.G. Wallace, Polym. Rev., 2013, **53**, 506-526.
40 M.J.C. Calagui, D.B. Senoro, C.-C. Kan, J.W.L. Salvacion, C.M. Futalan and M.-W. Wan, J. Hazard. Mater., 2014, **277**, 120-126.
41 A. Aluigi, F. Rombaldoni, C. Tonetti and L. Jannoke, J. Hazard. Mater., 2014, **268**, 156-165.
42 T.M. Mututuvari and C.D. Tran, J. Hazard. Mater., 2014, **264**, 449-459.
43 Y. Sun, Q. Yue, Y. Mao, B. Gao, Y. Gao and L. Huang, J. Hazard. Mater., 2014, **265**, 191-200.
44 K. Roy, P. Mondal, S.P. Bayen and P. Chowdhury, J. Macromolecul. Sci. A., 2012, **49**, 931-935.
45 N. Ballav, H.J. Choi, S.B. Mishra and A. Maity, J. Ind. Eng. Chem., 2014, **20**, 4085-4093.
46 G.-R. Xu, J.-N. Wang and C.-J. Li, Chem. Eng. J., 2012, **198–199**, 310-317.
47 N. Fiol, C. Escudero and I. Villaescusa, Bioresour. Technol., (2008), **99**, 5030-5036.
48 Y. Zhang, H.-L. Ma, J. Peng, M. Zhai and Z.-Z. Yu, J. Mater. Sci., 2013, **48**, 1883-1889.
49 J. Wang, K. Pan, E.P. Giannelis and B. Cao, RSC Adv., 2013, **3**, 8978-8987.

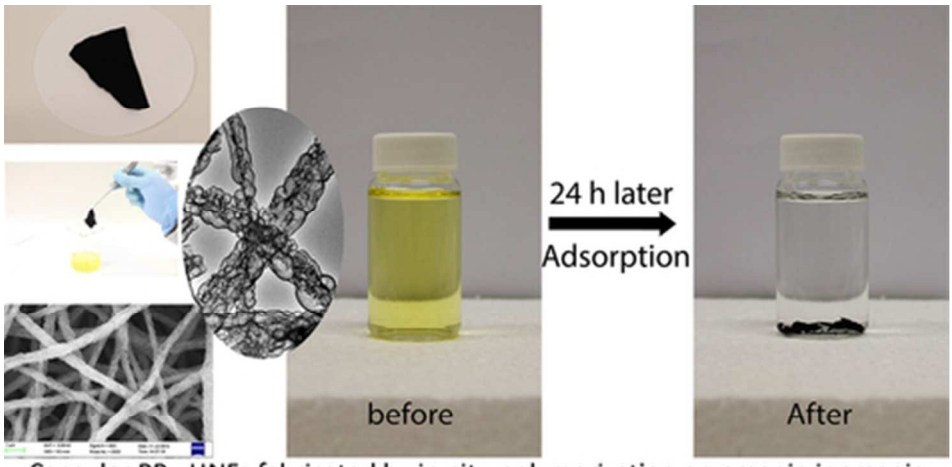

Capsular PPy-HNFs fabricated by in-situ polymerization on organic-inorganic templates showed an exceptional Cr (VI) adsorption capacity, up to 839.3 mg/g.

Graphical abstract
39x21mm (300 x 300 DPI)